

1 **Trackable and scalable LC-MS metabolomics data processing using asari**

2

3 Shuzhao Li*, Amnah Siddiq, Maheshwor Thapa, Shujian Zheng

4 Jackson Laboratory for Genomic Medicine, Farmington, CT 06032, USA

5

6 *Corresponding author, E-mail: shuzhao.li@jax.org

7

8 **Metabolomics holds the promise to measure and quantify small molecules**

9 **comprehensively in biological systems, and LC-MS (liquid chromatography coupled**

10 **mass spectrometry) has become the leading technology in the field. Significant**

11 **challenges still exist in the computational processing of data from LC-MS metabolomic**

12 **experiments into metabolite features, including provenance and reproducibility of the**

13 **current software tools. We present here asari, a new open-source software tool for LC-**

14 **MS metabolomics data processing. Asari is designed with a set of new algorithmic**

15 **framework and data structures, and all steps are explicitly trackable. It offers substantial**

16 **improvement of computational performance over current tools, and is highly scalable.**

17

18 In LC-MS metabolomics, a sample is scanned by mass spectrometer consecutively during the

19 chromatography, generating a time series of spectra, each containing a list of ions with mass to

20 charge ratio (m/z) and intensity values. The goal of data processing is to report a quantitative

21 value per metabolite feature per sample, which is a proxy of biological concentration. Multiple

22 software tools have been developed for LC-MS metabolomics data processing over the years,

23 and the most widely used are XCMS and MZmine (Smith et al, 2006, Katajamaa et al, 2006,

24 Pluskal et al, 2010, Du et al, 2020, Yu et al, 2013, Melamud et al, 2010, Rurik et al, 2020).

25 XCMS is also wrapped into numerous workflows and is the main choice in cloud environments

26 (Tautenhahn et al, 2012, Delabriere et al, 2021, Pang et al, 2021). Most these software tools

27 follow a similar framework: building ion chromatogram, detection of elution peaks, alignment of

28 retention time in liquid chromatography, and correspondence of peaks across samples. The

29 design was optimized when instrument resolution was limited and sample numbers were small,

30 not taking advantage of the ultrahigh resolution of modern instruments and the statistical

31 patterns in larger data. The correspondence step is error prone because a feature may only be

32 present as a high-quality peak in a subset of samples, and the computational problem is

33 complicated by missing data, low-quality data, m/z alignment and retention time alignment.

34

35 Asari uses a concept of "composite map" to look for peak patterns in cumulative data (**Figure**
36 **1A**). A specific form of a metabolite is observed in LC-MS as an elution peak. When the same
37 metabolites exist in multiple biological samples, such peaks are seen recurrently in nearly
38 identical m/z and similar elution profiles. When these corresponding signals from each sample
39 are superimposed and summed up, the observed peaks become representative of all samples
40 (**Figure 1B**). The "composite map" is a complete list of these composite chromatograms. With
41 this approach, peak detection is no longer required on individual samples. It can be done on the
42 composite map, then the peak area is looked up in each individual sample and reported as
43 feature intensity values (**Figure 1A**). This leads to a significant performance gain, by not
44 repeating the computational cost of peak detection on all individual samples. Because the
45 composite map has higher signals than any individual sample, the quality of peak detection is
46 often improved. Even a peak is only present in a single sample, it will be detected and reported
47 in asari, which is important to applications such as personalized medicine and exposomics.

48
49 The implementation of composite map is facilitated by a set of transparent data structures. Mass
50 tracks are extracted ion chromatograms spanning the full range of LC, therefore each mass
51 track has a unique m/z within a sample (**Figure S1**). A MassGrid records the alignment of mass
52 tracks across samples. A feature is defined at experiment level, and elution peaks are defined at
53 sample level. A metabolite may have multiple degenerate features due to isotopes, adducts,
54 neutral loss and fragments, which are grouped by an "empirical compound". An empirical
55 compound is a computational unit for a tentative metabolite, since the experimental
56 measurement may not separate compounds of identical mass (isomers). Asari explicitly links
57 mass track, peak, feature and empirical compound, so that each processing step can be traced
58 and verified. These data structures are exported as JSON or text tables. An interactive
59 dashboard can be launched after data are processed, to allow users to visually inspect data and
60 feature quality easily (**Figures S2, S3**).

61
62 The ability to verify feature quality is a priority in asari. Besides peak shape and signal-to-noise
63 ratio (SNR), we have implemented a set of selectivity metrics: mSelectivity is how distinct are
64 m/z measurements (**Figure 1C**), and cSelectivity is how distinct are chromatographic elution
65 peaks (**Figure 1D**). A derivative of mSelectivity is dSelectivity, applied to how distinct are
66 database records. In feature tables generated by asari, the values of SNR, cSelectivity and
67 peak shape are usually sufficient to judge the quality of LC-MS features.

68

69 We demonstrate the results of asari on four datasets generated in our lab (HZV029, MT02,
70 SZ22, BM21) and three public datasets (SLAW as described in Delabriere et al, 2021 as
71 LargeQE, ST001667 and ST001237). They are compared to XCMS, the current leading
72 software. The HZV029 dataset contains 268 data files, from two QC samples that were
73 analyzed repeatedly over 17 batches. The number of features detected in a LC-MS
74 metabolomics experiment is dependent on how parameters allow low-quality peaks to be
75 counted (Myer et al, 2017). Therefore, the comparison first focuses on features of high intensity,
76 and the majority of XCMS features are found in asari (912 out of 1091, **Figure 2A** left). When
77 the data are further filtered by 40% presence across files, all but 19 features from XCMS are
78 found in the result by asari (**Figure 2A** right). Investigation of these 19 features revealed that 10
79 were present in asari features that did not pass the average height of 1E6, and the remaining 9
80 features were not deemed of good quality (see Methods). The intensity values of the common
81 features are in good agreement (**Figure 2B**). Besides these data from Orbitrap platforms,
82 similar agreement is seen in Q-TOF data (**Figure S4**).

83

84 The MT02 dataset contains the widely used human plasma reference sample NIST SRM 1950.
85 The overall features in this sample detected by both asari and XCMS have consistent values
86 (**Figure 2C**). To establish the true positive features, we referred to the previously reported
87 metabolites in this sample (Simon-Manso et al, 2013), and curated a list of features that were
88 manually verified in raw data (**Table S1**). Both asari and XCMS successfully detected all these
89 39 “ground truth” features (**Figure 2D**). In the SZ22 dataset, ground truth was established by
90 credentialing in *E. coli* (similar to Mahieu et al, 2014). A subset of *E. coli* metabolites were
91 labeled by ¹³C isotope during the cell culture, and they were selected by elevated ¹³C/¹²C ratio
92 and manual inspection of raw data (**Table S2**). Asari successfully detected 71 out of 74 of these
93 credentialled features (**Figure 2E**). Two of the missed features were of low intensity and one of
94 incomplete elution peak. These data indicate that the feature detection by asari is at least on par
95 with XCMS performance.

96

97 Reproducibility of feature quantification (also called semi- or relative quantification, to distinguish
98 from targeted methods) is largely driven by experimental variations, while the processing
99 software plays a partial role. Because the HZV029 dataset contains many repeated
100 measurements of the same material, we calculated their pairwise Pearson correlations between
101 samples (**Figure 2F**) and coefficient of variation of features (**Figure 2G**) as metrics of
102 reproducibility. When features are binned by the asari quality metrics of SNR, peak shape and

103 cSelectivity, the top features show better reproducibility (**Figure 2F**). XCMS performed not as
104 well in these metrics of reproducibility, likely due to more missing values (not shown). Of note,
105 the more important contributions to reproducibility by asari reside in its trackable steps, few
106 parameters, transparently linked data structures and the visual dashboard where users can
107 easily verify results. In asari, the only parameter requiring user attention is the mass precision
108 (default at 5 part per million). This eliminates many reproducibility problems in complicated
109 parameter setting in other tools.

110
111 To further investigate the performance in quantification, we designed an experiment where
112 human plasma and vegetable juice were mixed by varying ratios (BM21 dataset, **Figure 3A**).
113 Therefore, a subset of features are expected to have their peak areas correlated with the mixing
114 ratio. Overall, 8,222 features were detected by both XCMS and asari in the BM21 dataset,
115 whereas asari has better quantification as indicated by more features with correlation coefficient
116 > 0.9 (**Figure 3B**).

117
118 To test the computational efficiency, multiple datasets were processed by both asari and XCMS,
119 and asari provides significant improvement of CPU time over XCMS by 1~2 orders of magnitude
120 (**Figure 3C**). When tested on the SLAW dataset using varying sample numbers, the CPU time
121 and memory use is mostly a linear function of sample numbers (**Figure 3D, E**). The results
122 indicate that the performance gap between XCMS and asari widens for larger studies. XCMS
123 can also become more complicated if it goes beyond simple workflows or large studies are
124 processed (Delabriere et al, 2021). The full SLAW dataset of > 2,000 samples was processed
125 by XCMS in the previous study on a cluster node of 15 CPU cores in 7~12 hours. Now it takes
126 asari ~1 hour on a regular laptop computer.

127
128 In summary, the development of asari has significantly contributed to the reproducible data in
129 metabolomics, by a full set of linked and transparent data structures in all processing steps. This
130 allows developers to trace, debug and optimize the process into the future. The end users can
131 navigate and verify features by interactive visualization of extracted ion chromatograms in asari
132 dashboard. Asari has delivered a new generation of computational performance, which is
133 necessary for the future growth of metabolomics. Asari has been mostly tested on Orbitrap
134 platforms. Community involvement will be important to cover the diverse platforms and methods
135 in metabolomics. Asari is free and open-source, and its modular design enables easy reuse of
136 the code for many tasks in computational metabolomics.

137 **Figures**

138

139 **Figure 1. Algorithmic designs and quality metrics in asari.**

140 A) Asari takes centroid mzML files as input, and build chromatograms for each as mass tracks.

141 To prioritize modern mass resolution, m/z alignment is performed first to form a MassGrid, aided
142 by isotopic landmarks. The retention time (RT) alignment is based on LOWESS regression,
143 using a subset of high-quality elution peaks. Elution peak detection is performed on the
144 composite mass tracks, and feature table is generated by looking up the corresponding peak
145 areas in each individual sample. Annotation groups degenerate features into empirical
146 compounds, and reference databases are used to match the m/z values in empirical
147 compounds.

148 B) The "composite map" is a representation of data from all samples, by adding up the signals
149 in corresponding mass tracks after RT alignment.

150 C) Illustration of mSelectivity (y-axis) as a function of neighboring m/z values. Each dot
151 represents a m/z feature, and its mSelectivity value depends on the horizontal distance to
152 neighbor features. The error in matching m/z values is modeled as a gaussian distribution
153 dependent on mass precision, and mSelectivity is low when a feature has neighbors with close
154 m/z values.

155 D) Chromatographic peak selectivity (cSelectivity) is defined by the fraction of the data points in
156 all peaks above 1/2 this peak height and all data points above 1/2 this peak height. cSelectivity
157 is 1 when the chromatogram has no noise above the half height of any peak.

158

159 **Figure 2. Evaluation of asari feature detection and reproducibility.**

160 A) Overlap between asari and XCMS on HZV029 dataset. Similar parameters were applied to
161 both software tools: min intensity 1000, 5 ppm mass accuracy. In XCMS, centwave window is
162 set at (1, 30), min peak height at 1E6. Because asari has no minimal peak height requirement
163 on individual samples, the features are filtered by average peak height above 1E6, which is
164 more stringent and results in fewer features. The common (matched within 5 ppm and 10
165 seconds) and unique numbers of features are shown on the left. When further filtered by the
166 presence in at least 40% of samples, the common and unique numbers of features are shown
167 on the right. The common numbers differ between two tools because of decisions in peak
168 splitting or merging.

169 B-C) Scatter plot of the \log_2 peak areas of common features between the two tools. B)
170 corresponds to the right panel in A) on a random sample in HZV029. C) corresponds to a NIST
171 SRM 1950 reference sample. R value shown is correlation coefficient in Pearson correlation.
172 D-E) Detected features on ground truth datasets in NIST SRM 1950 reference sample (D) and
173 credentialed E. coli samples (E).
174 F) Of HZV029 asari features, 4,746 have $\text{SNR} > 1\text{E}3$, among which 1,187 are denoted as
175 medium quality for peak shape < 0.95 . A set of 1,005 features with $\text{SNR} > 1\text{E}4$, peak shape $>$
176 0.95 and cSelectivity > 0.99 are denoted as top quality. The heatmaps show the reproducibility
177 of randomly selected 32 Qstd samples, colored by their Pearson correlation coefficients.
178 G) Reproducibility across 17 batches is shown by the distribution of coefficients of variation of
179 the top features and medium features in all 184 Qstd samples. The feature data are not
180 normalized or batch corrected.

181

182 **Figure 3. Evaluation of quantification and computational performance.**

183 A) Design of the BM21 dataset, by varying mix ratios between human plasma and vegetable
184 juice. A well quantified metabolite is expected to show good correlation between the mixing
185 ratios and the reported peak areas, as exemplified by the feature on top (m/z 189.1232, 159
186 seconds). Asari calculates peak area differently from XCMS, resulting in higher values in
187 Orbitrap data.
188 B) Overall quantification results in the BM21 dataset, shown as feature numbers binned by
189 Pearson correlation coefficients between peak areas and sample mixing ratios.
190 C) Computational performance in user CPU time (equivalent to single core) by asari and XCMS
191 on different datasets (sample numbers show in parentheses on X-axis). Y-axis is in \log_{10} scale.
192 The annotation step is included in asari not in XCMS.
193 D-E) CPU time and wall clock time (D) and memory (E) used by asari and XCMS on the SLAW
194 dataset using varying number of samples.

195

196

197

198

199 **Supplements**

200

201 **Figure S1 Illustration of mass tracks in a single sample.** The region has 7 mass tracks
202 marked by green boxes spanning horizontally, each of a unique m/z value. A peak is detected
203 from the track indicated by the yellow arrow.

204

205 **Figure S2. Screen shot of asari Dashboard: feature browser.**

206

207 **Figure S3. Screen shot of asari Dashboard, view of a mass track.**

208

209 **Figure S4. Consistency of feature peak areas shown on an Agilent Q-TOF dataset**
210 **(ST001667).**

211

212 **Table S1. Manually verified true features in NIST SRM 1950.**

213 Potentially redundant isomers are colored. Since the goal here is not metabolite identification,
214 but to test if software detects the presence of a real feature, the isomers are not distinguished in
215 experimental data.

216

217 **Table S2. Manually verified true features in credentialed E. coli samples.**

218

219

220

221

222

223

224 **References:**

225
226 Delabriere, A., Warmer, P., Brennsteiner, V. and Zamboni, N., 2021. SLAW: A Scalable and
227 Self-Optimizing Processing Workflow for Untargeted LC-MS. *Analytical Chemistry*,
228 93(45), pp.15024-15032.

229
230 Du, X., Smirnov, A., Pluskal, T., Jia, W. and Sumner, S., 2020. Metabolomics data
231 Preprocessing using ADAP and MZmine 2. In *Computational Methods and Data*
232 *Analysis for Metabolomics* (pp. 25-48). Humana, New York, NY.

233
234 Katajamaa, M., Miettinen, J. and Orešič, M., 2006. MZmine: toolbox for processing and
235 visualization of mass spectrometry based molecular profile data. *Bioinformatics*, 22(5),
236 pp.634-636.

237
238 Li, S., Sullivan, N.L., Roush, N., Yu, T., Banton, S., Maddur, M.S., McCausland, M., Chiu, C.,
239 Canniff, J., Dubey, S. and Liu, K., 2017. Metabolic phenotypes of response to
240 vaccination in humans. *Cell*, 169(5), pp.862-877.

241
242 Mahieu, N.G., Huang, X., Chen, Y.J. and Patti, G.J., 2014. Credentialing features: a platform to
243 benchmark and optimize untargeted metabolomic methods. *Analytical Chemistry*,
244 86(19), pp.9583-9589.

245
246 Melamud, E., Vastag, L. and Rabinowitz, J.D., 2010. Metabolomic analysis and visualization
247 engine for LC- MS data. *Analytical chemistry*, 82(23), pp.9818-9826.

248
249 Myers, O.D., Sumner, S.J., Li, S., Barnes, S. and Du, X., 2017. Detailed investigation and
250 comparison of the XCMS and MZmine 2 chromatogram construction and
251 chromatographic peak detection methods for preprocessing mass spectrometry
252 metabolomics data. *Analytical Chemistry*, 89(17), pp.8689-8695.

253
254 Pang, Z., Chong, J., Zhou, G., de Lima Morais, D.A., Chang, L., Barrette, M., Gauthier, C.,
255 Jacques, P.É., Li, S. and Xia, J., 2021. MetaboAnalyst 5.0: narrowing the gap between
256 raw spectra and functional insights. *Nucleic acids research*, 49(W1), pp.W388-W396.

257
258 Pluskal, T., Castillo, S., Villar-Briones, A. and Orešič, M., 2010. MZmine 2: modular framework
259 for processing, visualizing, and analyzing mass spectrometry-based molecular profile
260 data. *BMC bioinformatics*, 11(1), pp.1-11.

261
262 Rurik, M., Alka, O., Aicheler, F. and Kohlbacher, O., 2020. Metabolomics data processing using
263 OpenMS. *Computational Methods and Data Analysis for Metabolomics*, pp.49-60.

264
265 Simon-Manso, Y., Lowenthal, M.S., Kilpatrick, L.E., Sampson, M.L., Telu, K.H., Rudnick, P.A.,
266 Mallard, W.G., Bearden, D.W., Schock, T.B., Tchekhovskoi, D.V. and Blonder, N., 2013.
267 Metabolite profiling of a NIST Standard Reference Material for human plasma (SRM
268 1950): GC-MS, LC-MS, NMR, and clinical laboratory analyses, libraries, and web-based
269 resources. *Analytical chemistry*, 85(24), pp.11725-11731.

270
271 Smith, C.A., Want, E.J., O'Maille, G., Abagyan, R. and Siuzdak, G., 2006. XCMS: processing
272 mass spectrometry data for metabolite profiling using nonlinear peak alignment,
273 matching, and identification. *Analytical chemistry*, 78(3), pp.779-787.

274

275 Tautenhahn, R., Patti, G.J., Rinehart, D. and Siuzdak, G., 2012. XCMS Online: a web-based
276 platform to process untargeted metabolomic data. *Analytical chemistry*, 84(11), pp.5035-
277 5039.

278

279 Wishart, D.S., 2020. Metabolomic data exploration and analysis with the human metabolome
280 database. In *Computational Methods and Data Analysis for Metabolomics* (pp. 165-184).
281 Humana, New York, NY.

282

283 Yu, T., Park, Y., Li, S. and Jones, D.P., 2013. Hybrid feature detection and information
284 accumulation using high-resolution LC-MS metabolomics data. *Journal of proteome
285 research*, 12(3), pp.1419-1427.

286

287

288 **Data availability:** The datasets MT02 and SZ22 are available at <https://github.com/shuzhao->
289 li/data. The BM21 and HZV029 datasets are in the submission process to Metabolomics
290 Workbench (<https://www.metabolomicsworkbench.org/>), and will be made publicly available at
291 the time of publication.

292 The public datasets used in this work are under Study IDs ST001667 and ST001237 on
293 Metabolomics Workbench. The large SLAW dataset was retrieved from MassIVE by study ID
294 MSV000086486 (Delabriere et al, 2021).

295

296 **Code availability:** The asari source code is available at GitHub, <https://github.com/shuzhao->
297 li/asari, and as a Python package via <https://pypi.org/project/asari-metabolomics/>.

298

299 **Acknowledgements:** This work was in parted funded by NIH grants (to SL) U01 CA235493
300 (NCI) and R01 AI149746 (NIAID).

301

302 **Author contributions:** S.L. designed the study, wrote the asari software and the manuscript.
303 A.S. and S.L. performed data analysis and software testing. M.T. performed the experiments of
304 HZV029, MT02 and BM21. S.Z. performed the experiment of SZ22.

305

306

307 **Methods**

308

309 **Software design of asari.** Asari is written in Python 3, and can be used as a standalone
310 command line tool or imported as a package. Its library dependency includes numerical
311 computing via numpy and scipy, data wrangling via pandas, and visualization via panel and
312 hvplot. Pymzml is used to parse mzML format. Data structures, annotation, search and chemical
313 calculation make use of our supporting packages metDatamodel, mass2chem and jms-
314 metabolite-services. Implementation of new and previous algorithms was coded from ground up,
315 where numerous details contributed to the computing speed, e.g., discrete mathematics is
316 preferred over continuous curves, and intermediary indexing and caches are employed.
317 Processed mass tracks are cached on disk to reduce memory footprint. Mass tracks are
318 explicitly linked with features and peaks, and the information is exported as JSON in asari
319 output. The quality metric mSelectivity is used internally and not exported by default. The
320 annotation and search functions are generic to accommodate reference databases, and the
321 default is HMDB (Wishart 2020).

322

323 **Evaluation of feature detection and computational performance.** The features from different
324 software tools in the same data are considered matched when their m/z values are within 5 ppm
325 and retention times are within 10 seconds. The results from XCMS did not use peak filling,
326 which often creates artifacts. The merging of adjacent peaks in XCMS is dependent on input
327 parameters, and often resulted more split peaks than the results in asari. The 9 XCMS features
328 that were not accepted by asari (Figure 2A) are (m/z @ retention time in seconds):
329 129.1022@25, 28.0197@17, 210.9937@16, 174.1854@23, 256.2999@23, 156.1133@14,
330 129.1023@13, 120.0808@15, 100.1121@15.

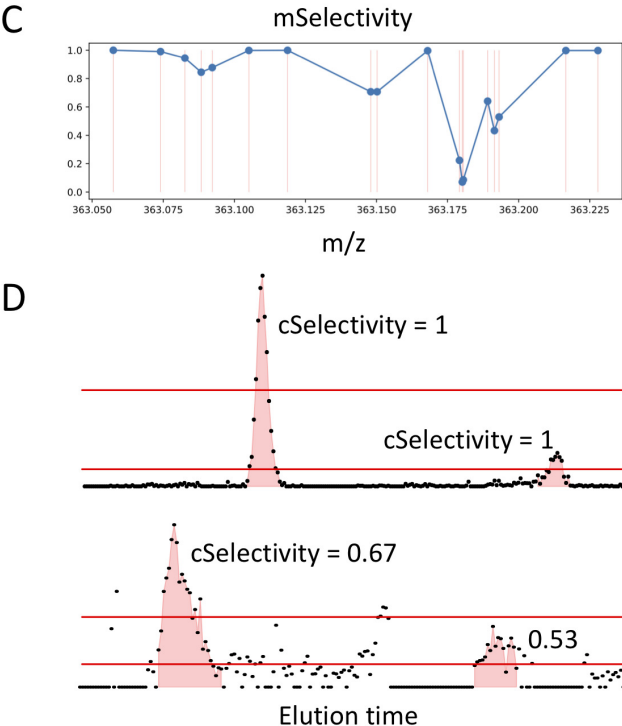
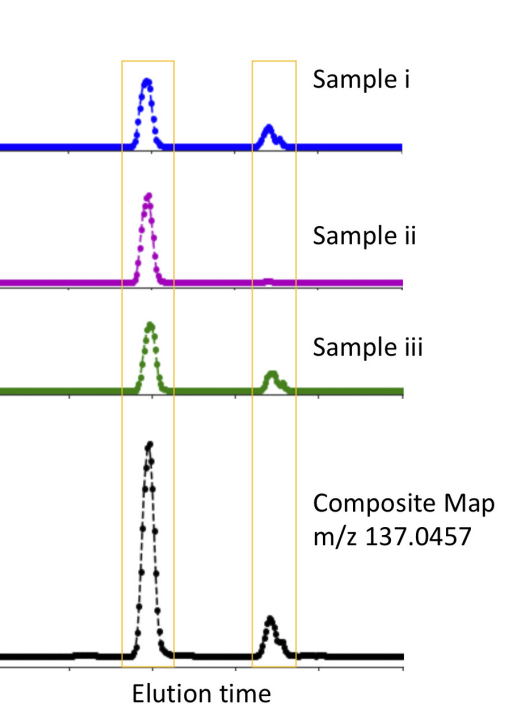
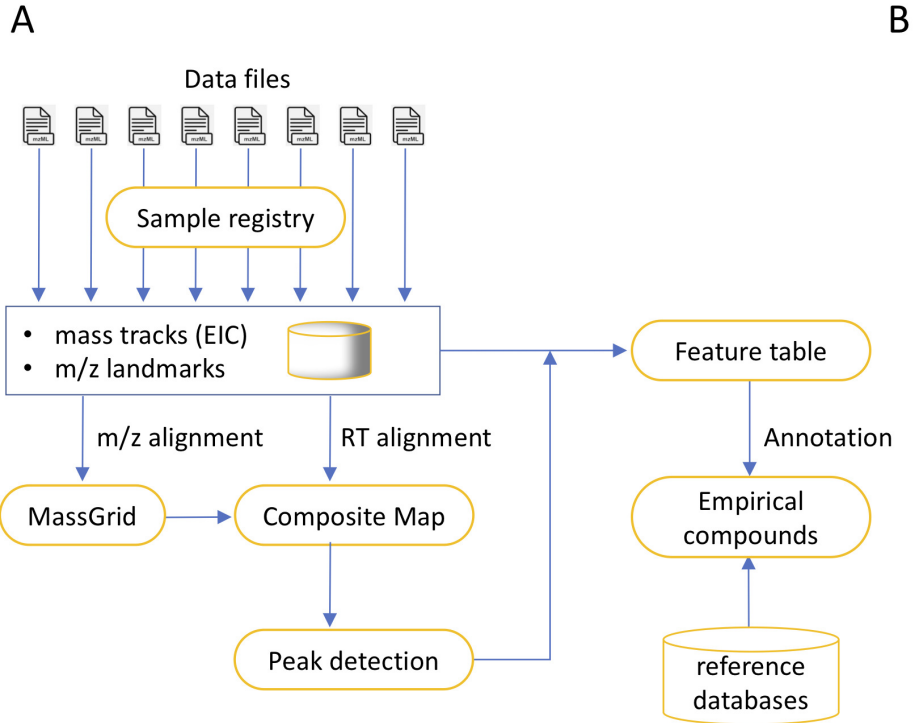
331 The “ground truth” features in the NIST SRM 1950 sample were manually verified and counted
332 as 39 true positive m/z features. The reported isomers are not distinguished here since our
333 retention time is not comparable to the previous publication. A positive match to either asari or
334 XCMS results requires a feature to be within 5 ppm. For the credentialed *E. coli* samples, a
335 feature is considered to be true positive when a) it is present in all six samples, b) presence of
336 the isotopic peak by 1.003355 m/z difference at the same retention time, c) the $^{12}\text{C}/^{13}\text{C}$ ratio > 1
337 in the unlabeled samples, and d) the $^{12}\text{C}/^{13}\text{C}$ ratio is > 2 -fold higher in the labeled samples than
338 unlabeled samples. The difference from the Mahieu et al (2014) paper was due to that we
339 analyzed the labeled and unlabeled samples separately, while the previous work mixed them at
340 specific ratios.

341 The evaluation of computational performance was performed on a desktop computer with Intel
342 i7-8809G CPU and 32 GB of memory, running Mint Linux 20.2. The asari version was 1.9.2.
343 The XCMS version was 3.18.0. The R script for XCMS is provided in asari repository
344 (<https://github.com/shuzhao-li/asari>) under doc/ directory. The time and memory use was
345 measured by `/usr/bin/time -p`, and “User time” was used as CPU time (equivalent to CPU time
346 used on a single core).

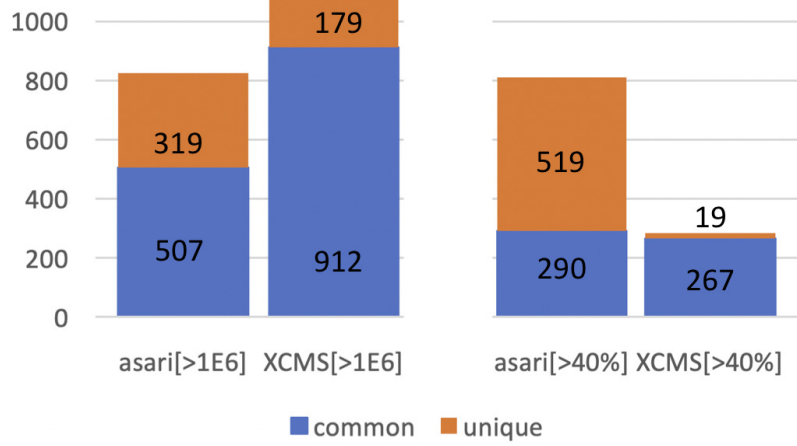
347

348 **LC-MS metabolomics experiments.** The human plasma samples used in this study were a
349 pooled deidentified QC sample in a vaccination cohort, NIST SRM 1950 (https://www-s.nist.gov/srmors/view_detail.cfm?srm=1950), and a commercial reference sample Qstd (Sterile
350 Filtered Human Plasma (K2) EDTA, Equitech Bio, Inc. KERRVILLE, TEXAS). The BM21
351 experiment included a serial mixture of human plasma (Qstd) and vegetable juice, at the ratio of
352 1024:1, 256:1, 64:1, 16:1, 4:1, 1:1, 1:4, 1:16, 1:64, 1:256 and 1:1024. Along with the 11 serial
353 mixture samples, 100% vegetable juice and 100% plasma were also included. All samples were
354 analyzed in triplicates, while one replicate was used for data analysis in this study for simplicity.
355 The dry extracts of unlabeled and ¹³C labeled *E. coli* (Cambridge Isotope Laboratories, Inc.;
356 Catalog number: MSK-CRED-DD-KIT) were reconstituted in 100 µL of ACN/H₂O (1:1, v/v) then
357 sonicated (10 mins) and centrifuged (10 mins at 13,000 rpm and 4°C) before overnight
358 incubation at 4°C. The supernatant for each ¹²C/¹³C *E. coli* extract was collected and then
359 prepared for LC-MS analysis. These samples were run in triplicates.
360 Metabolites extraction was carried out by protein precipitation technique using extraction
361 solvent, acetonitrile:methanol (8:1, v/v) containing 0.1% formic acid and isotope labelled
362 Trimethyl-13C3]-caffeine, [13C5]-L-glutamic acid, [15N2]-Uracil, [15N,13C5]-L-methionine,
363 [13C6]-D-glucose and [15N]-L-tyrosine as spike-in controls. 30 µL of plasma sample was taken
364 and 60 µL of extraction solvent was added. Extraction blanks were also prepared to remove
365 features of non-biological origins. All samples were vortexed and incubated with shaking at
366 1000 rpm for 10 min at 4°C followed by centrifugation at 4°C for 15 min at 15,000 rpm. The
367 supernatant was transferred into mass spec vials and 2 µL injected into UHPLC-MS.
368 All samples were maintained at 4 °C in the autosampler, and analyzed using a Thermo
369 Scientific Orbitrap ID-X Tribid Mass Spectrometer coupled to a Thermo Scientific Transcend LX-2
370 Duo UHPLC system, with a HESI ionization source, using positive and negative ionizations. The
371 MS settings are: spray voltage, 3500 V; sheath gas, 45 Arb; auxiliary gas, 20 Arb; sweep gas, 1
372 Arb; ion transfer tube temperature, 325 °C; vaporizer temperature, 325 °C; mass range, 80-

374 1000 Da; maximum injection time, 100 ms. The resolution was set at 120,000 in the HZV029
375 experiment, 60,000 in the BM21 and SZ22 experiments.
376 Data were acquired using hydrophilic interaction liquid chromatography (HILIC) positive and
377 reversed phase (RP) negative polarities in full scan mode with mass resolution of 120,000
378 simultaneously. An AccucoreTM-150-Amide HILIC column (2.6 μ m, 2.1 mm x 50 mm) and a
379 Hypersil GOLDTM RP column (3 μ m, 2.1 mm x 50 mm) maintained at 45 °C were used for
380 chromatographic separation. 0.1% formic acid in water and 0.1% formic acid in acetonitrile were
381 used as mobile phase A and B respectively for RP acquisition. 10 mM ammonium acetate in
382 acetonitrile:water (95:5, v/v) with 0.1% acetic acid as mobile phase A and 10 mM ammonium
383 acetate in acetonitrile:water (50:50, v/v) with 0.1% acetic acid as mobile phase B were used for
384 HILIC method. For HILIC acquisition, following gradient was applied at a flow rate of 0.55
385 ml/min: 0-0.1 min: 0% B, 0.10-5.0 min: 98% B, 5.00-5.50 min: 0% B and 4.5 min for cleaning
386 and equilibration of column. For RP column, following gradient was applied at a flow rate of 0.4
387 ml/min: 0-0.1 min: 0% B, 0.10-1.9 min: 60% B, 1.9-5.0 min: 98% B, 5.00-5.10 min: 0% B and 4.9
388 min cleaning and column equilibration. The chromatographic run time was 5 min followed by 5
389 min washing step after each sample.

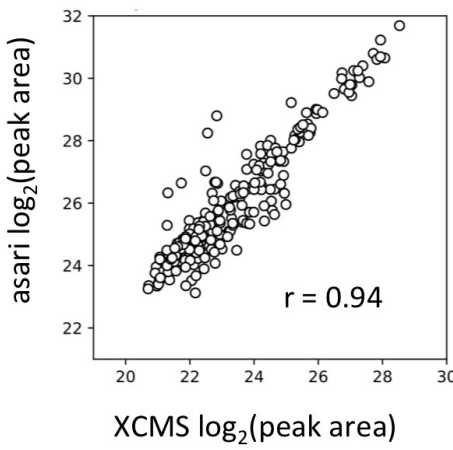


A



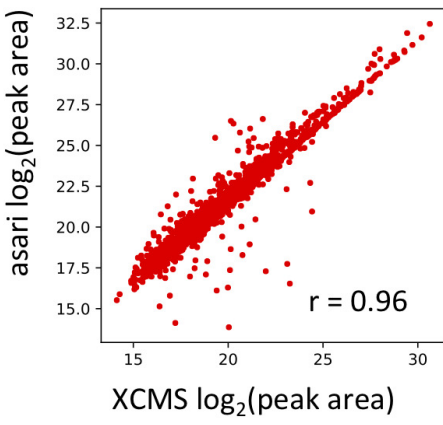
B

HZV029



C

NIST SRM1950



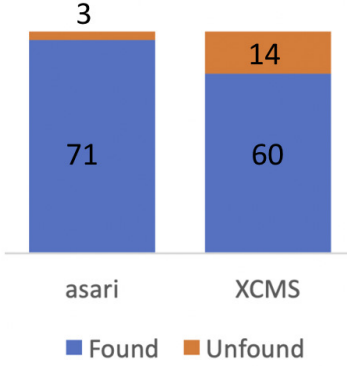
D

NIST SRM1950

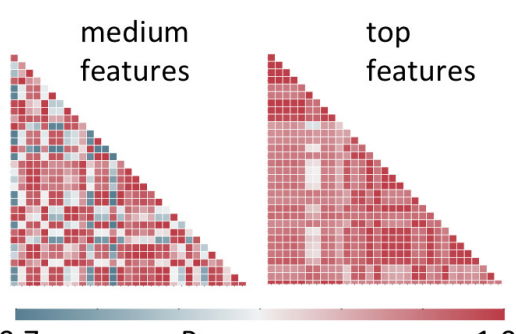


E

Credentialed E. coli



F



G

